Supporting Information

Development of New Quinoline-Triazole Based Hybrids: Synthesis, Nano-Encapsulation, DFT Calculations, and Evaluation of Antidiabetic and Antioxidant Activity

Fatma M. Elhalmoushy [a], Mohamed N. Abd Al Moaty [a,b], Alaa S. Hegazy [c], Saied M. Soliman [a], Mazen Sherif [d], Doaa A. Ghareeb [d,e,f], Mohamed Hagar *[a] and Manar Ahmed Fouad *[a].

[a] *Department of Chemistry, Faculty of Science, Alexandria University, P.O. Box 426, Alexandria 21321, Egypt. Email: M. Hagar, mohamed.hagar@alexu.edu.eg ; M.A. Fouad, manar.ahmed@alexu.edu.eg*

[b] *Chemistry Department, Faculty of Advanced Basic Science, Alamein International University, Alamein City, Matrouh Governorate, Egypt.*

[c] *Department of Medical Laboratory Technology, Faculty of Applied Health Sciences Technology, Pharos University in Alexandria, Alexandria, Egypt.*

[d] *Bio-screening and Preclinical Trial Lab, Biochemistry Department, Faculty of Science, Alexandria University, Alexandria, Egypt.*

[e] *Center of Excellence for Drug Preclinical Studies (CE-DPS), Pharmaceutical and Fermentation Industry Development Center, City of Scientific Research & Technological Applications (SRTA-city), New Borg El Arab, Alexandria, Egypt.*

[f] *Research Projects Unit, Pharos University in Alexandria, Canal El Mahmoudia Street, Beside Green Plaza Complex, 21648, Alexandria, Egypt.*

Contents **Page**

1. FTIR, NMR, and HRMS Spectra of compounds 5 and 6.

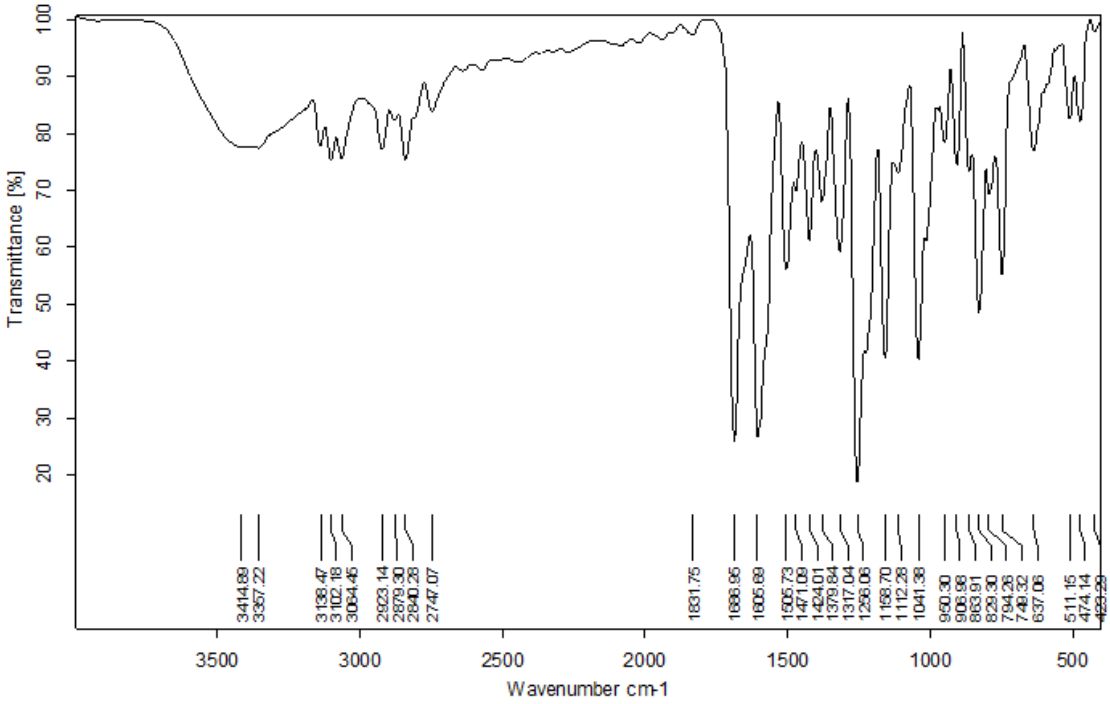

Figure S1. FTIR (KBr) of **5**.

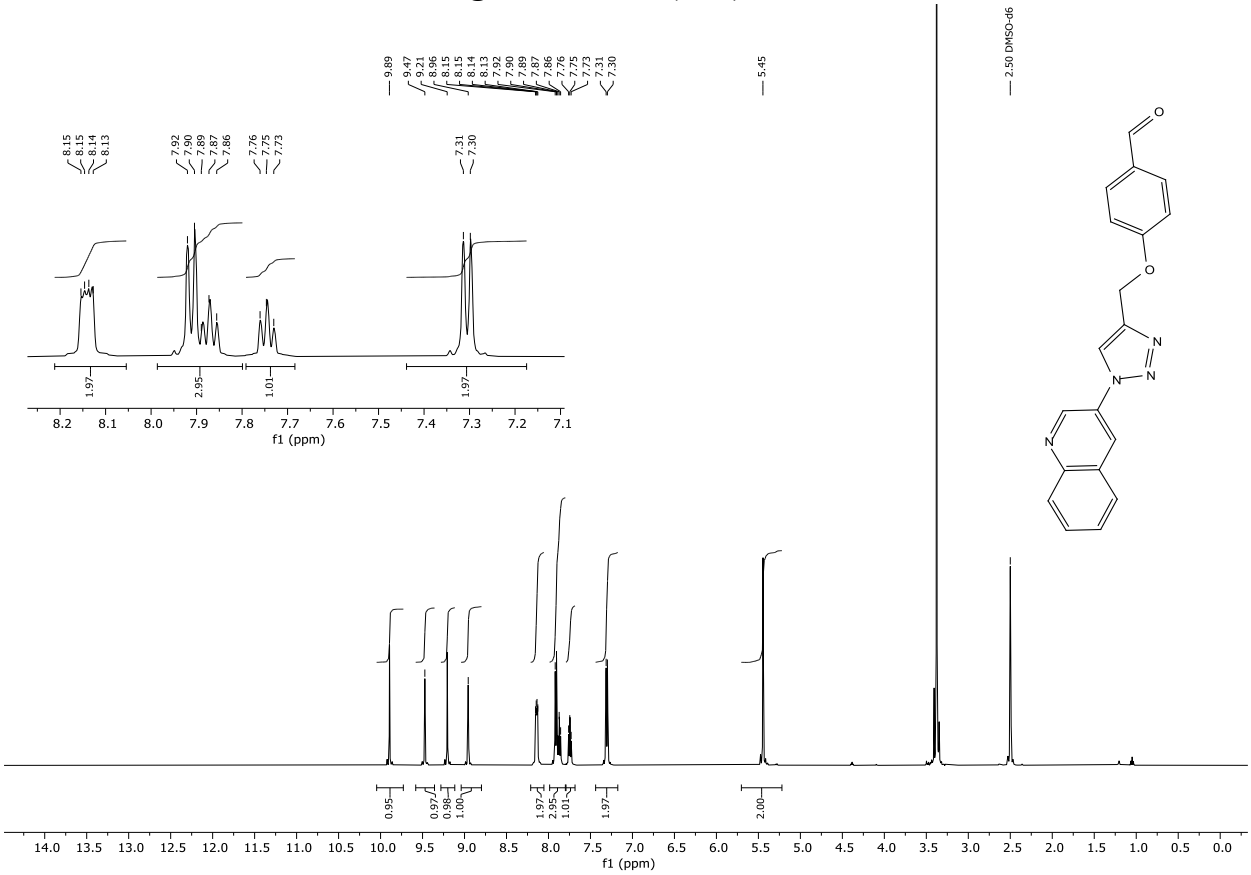

Figure S2. ^{1}H NMR of **5** (500 MHz, DMSO-d_6).

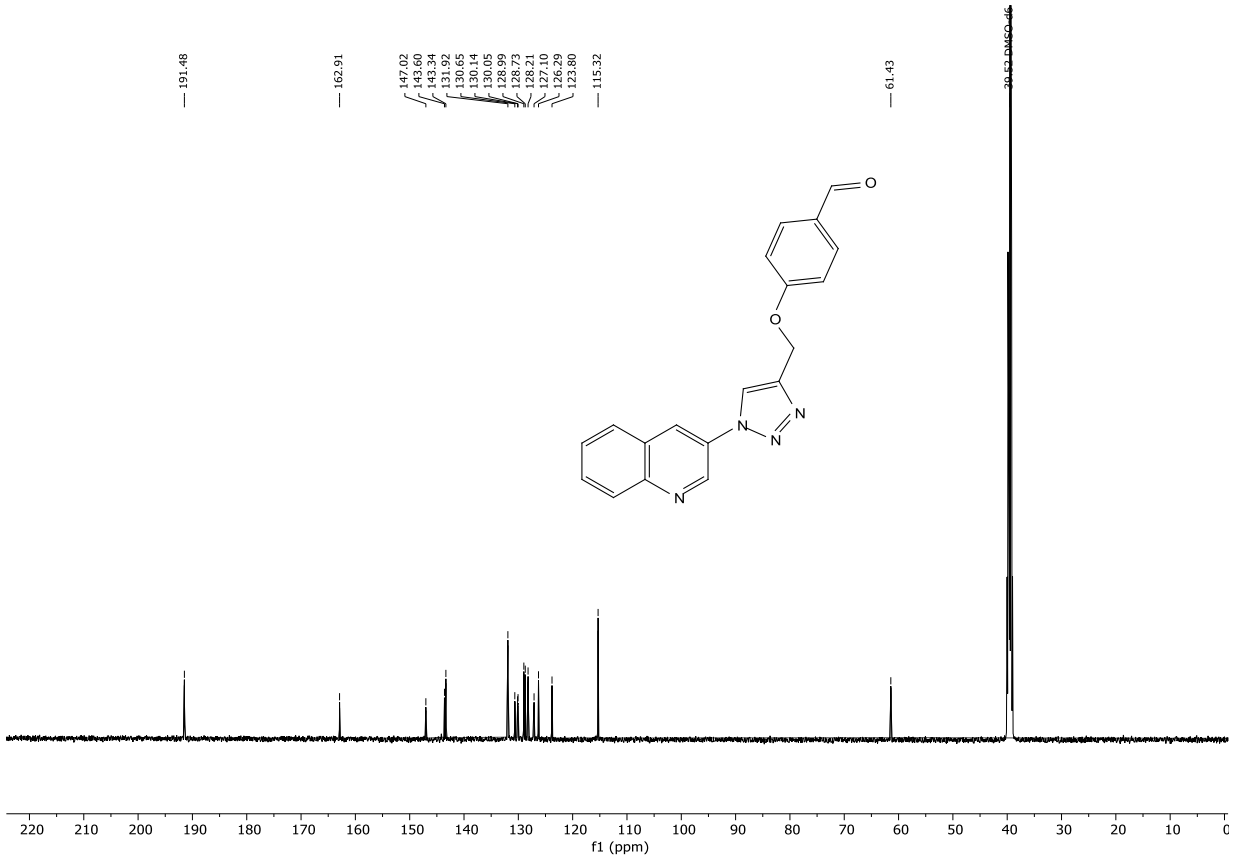

Figure S3. ^{13}C NMR **of 5** (125 MHz, DMSO-d_6).

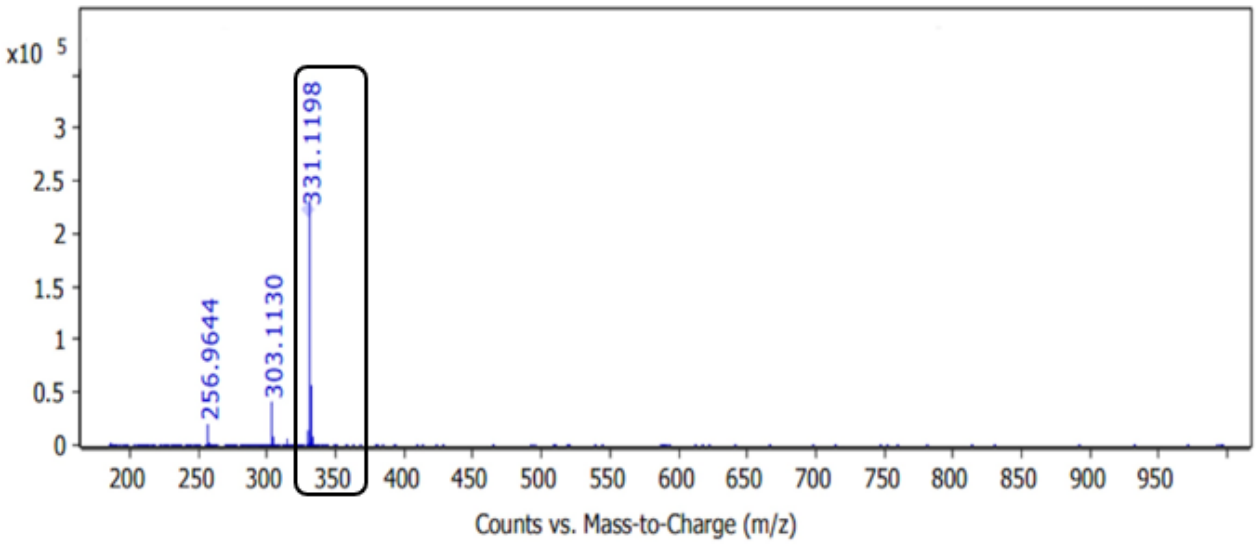

Figure S4. HRMS (ESI$^+$) of compound **5**.

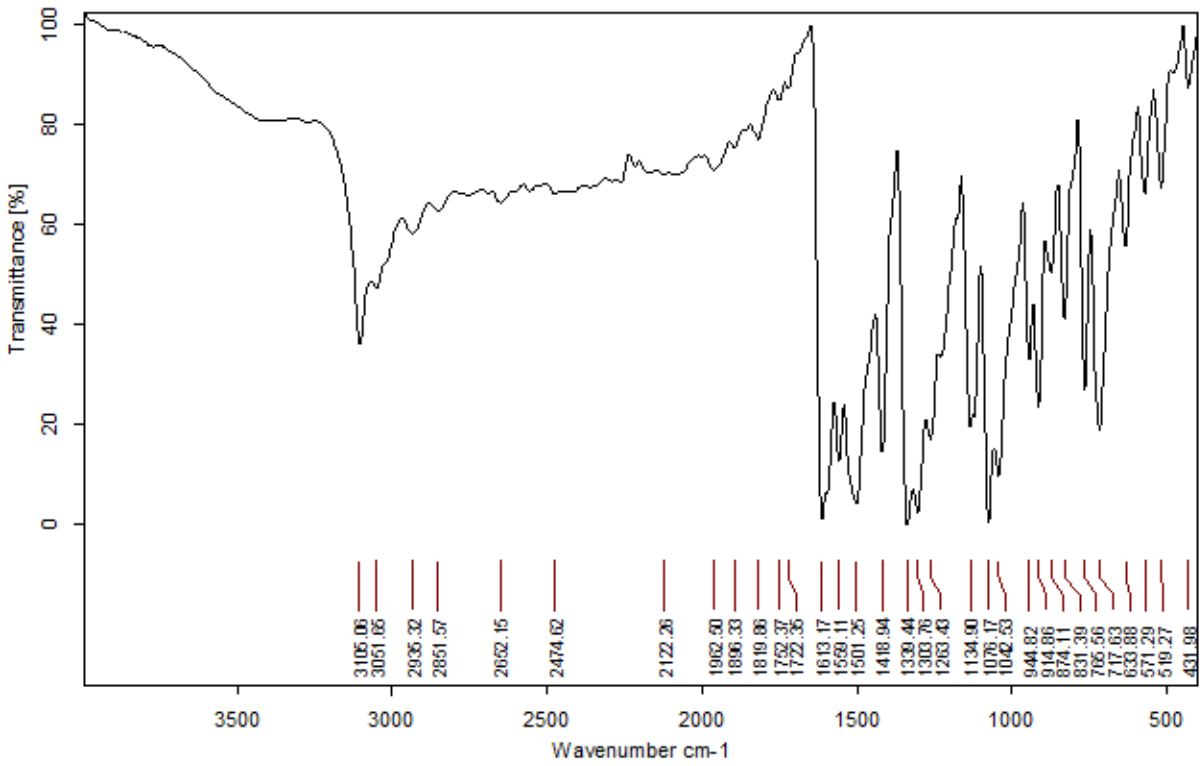

Figure S5. FTIR (KBr) of **6**.

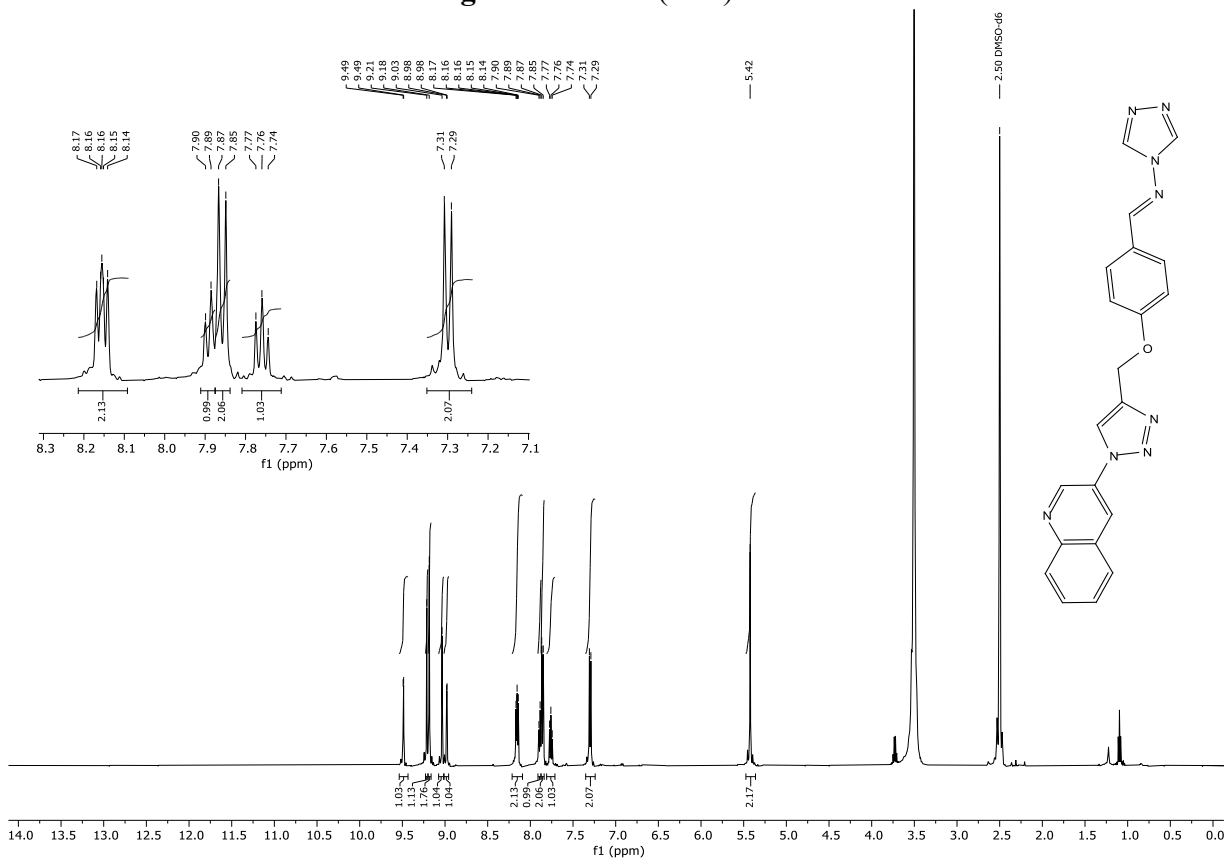

Figure S6. ^{1}H NMR of **6** (500 MHz, DMSO-d_6).

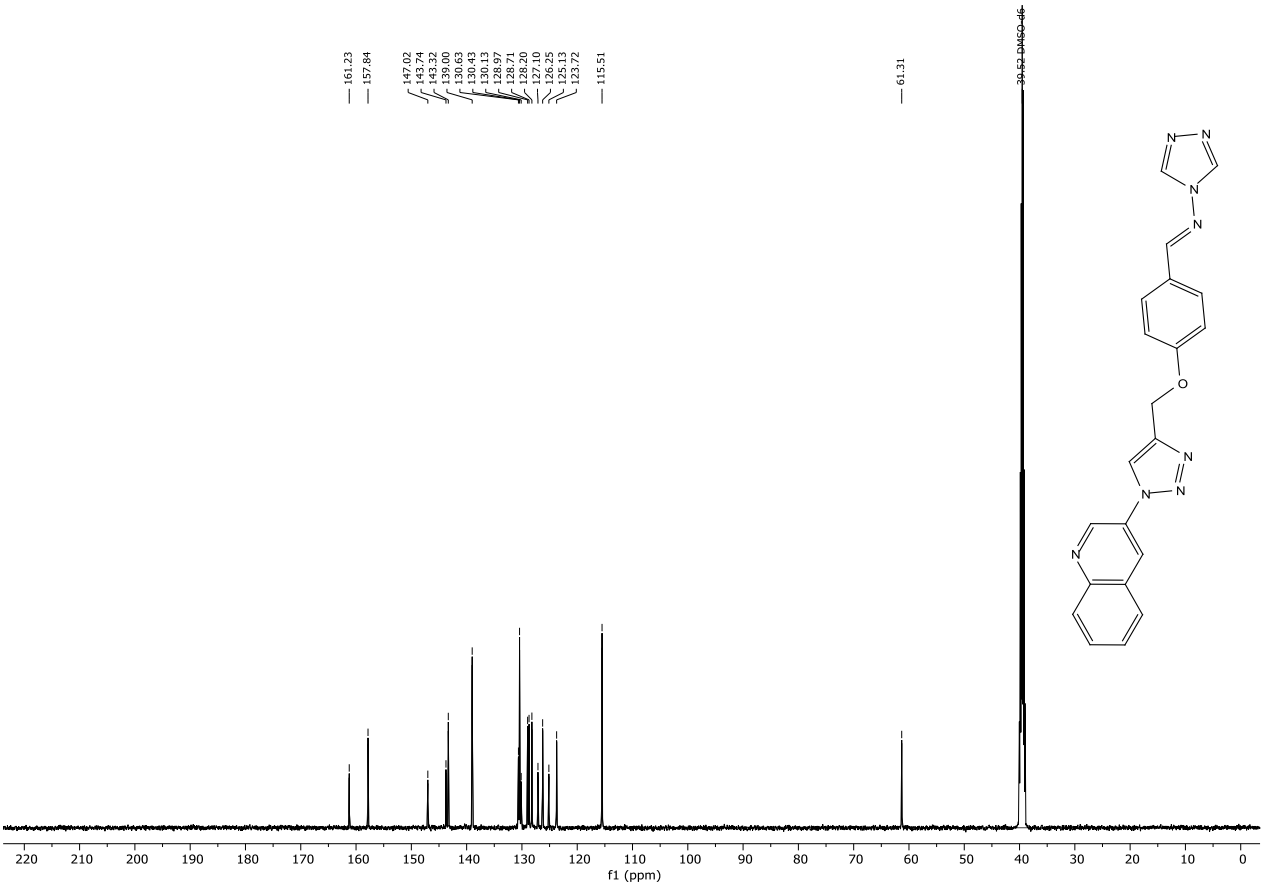

Figure S7. ^{13}C NMR of **6** (125 MHz, DMSO-d_6).

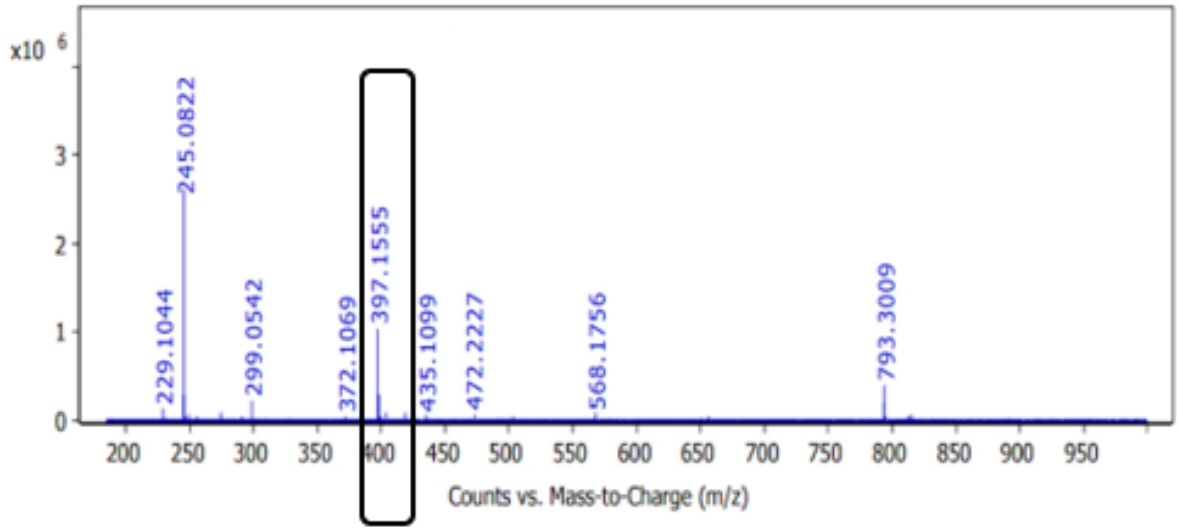

Figure S8. HRMS (ESI$^+$) of compound **6**.

2. General Information

Unless otherwise stated, all chemicals and solvents were of analytical grade and purchased from Sigma-Aldrich. The progress of all chemical reactions was monitored using Merck TLC precoated silica gel 60 F254 aluminum sheets (20 × 20 cm, Merck KGaA, Darmstadt, Germany). The chromatograms were visualized under UV light at 254 nm. Melting points were determined using a Büchi model B-545 apparatus (Büchi Corporation, Flawil, Switzerland) and were uncorrected. FTIR spectra were recorded with a PerkinElmer 1600 series infrared spectrophotometer (Waltham, MA, USA) using potassium bromide (KBr) pellets, and absorption bands ($\bar{\nu}_{max}$) were reported in wavenumbers (cm^{-1}). ^{1}H and ^{13}C NMR spectra were recorded at 500 and 125 MHz, respectively, using a JNM-ECZ500R/S1 spectrometer (JEOL) in DMSO-d_6, the deuterated solvent served as an internal deuterium lock, with tetramethylsilane (TMS) as an internal standard for protons and solvent signals. Chemical shift (δ) values are reported in ppm, and coupling constants (J) are given in Hz. High-resolution mass spectra (HRMS) were obtained using an LC/Q-TOF 6530 mass spectrometer (Agilent Technologies, Santa Clara, CA, USA) equipped with an electrospray ionization (ESI) source that operated in positive ion mode. Accurate mass measurements were provided as mass-to-charge ratios (m/z). TEM imaging of Chitosan nano particles was performed on a JEOL JEM-1400 Plus. Zeta potential measurements were recorded with Zetasizer Nano ZS90/ZEN3600 (Malvern Instruments, UK).

2.1. Synthesis of compounds (2) and (4)

2.1.1. Synthesis of 3-azidoquinoline (2)

Compound **2** was prepared according to a previously reported procedure.[1] A solution of 3-aminoquinoline (**1**) (3.50 mmol, 1.0 equiv.) in 10% aqueous hydrochloric acid (4 mL) was prepared and cooled in an ice bath. An aqueous solution of sodium nitrite (3.10 mmol, 1.1 equiv., 10 mL of distilled water) was added gradually to this solution, and the mixture was stirred in the ice bath for 1 h. Subsequently, an aqueous solution of sodium azide (3.10 mmol, 1.1 equiv., 10 mL of distilled water) was added dropwise, and the reaction mixture was stirred in the ice bath for an additional hour. After completion, the reaction mixture was neutralized with aqueous $NaHCO_3$ solution to precipitate the product which was collected by filtration, and washed with water to afford azide **2** as a pale-yellow solid (3.46 mmol, 98%). The spectral data of the synthesized compound were consistent with those reported in literature.

2.1.2. Synthesis of 4-(prop-2-yn-1-yloxy)benzaldehyde (4)

Compound **4** was prepared according to a previously reported procedure.[2] A mixture of 4-hydroxybenzaldehyde (**3**) (4.10 mmol, 1.0 equiv.) and propargyl bromide (4.10 mmol, 1.0 equiv.) in the presence of anhydrous K_2CO_3 (4.90 mmol, 1.2 equiv.) was refluxed in dry acetone (20 mL) for 4 h. The reaction progress was monitored by TLC until completion. The reaction mixture was then cooled to room temperature, filtered, and the solid residue was washed with acetone. The combined filtrates were concentrated, and the crude product was recrystallized from ethanol to afford 4-(prop-2-yn-1-yloxy)benzaldehyde (**4**) as colorless crystals (4.00 mmol, 98%). The spectral data of the synthesized compound were consistent with those reported in literature.

2.2. Determination of encapsulation efficiency (EE%)

The encapsulation efficiency (EE%) of the prepared chitosan nanoformualtions was determined indirectly by quantifying the amount of unencapsulated (free) drug present in the supernatant according to the reported procedure.[3] Calibration curves for compounds **5** and **6** were established by preparing stock solutions in dimethyl sulfoxide (DMSO), followed by appropriate serial dilutions. The absorbance of each concentration was measured at the predetermined maximum absorption wavelength (λ_{max} = 283 nm for compound **5** and 305 nm for compound **6**), and calibration plots were constructed accordingly. The electronic absorption spectra of the studied compounds were recorded over the wavelength range of 190-800 nm using a double-beam UV-Vis spectrophotometer (T80+ UV/Vis, PG Instruments Ltd., UK).

For EE% determination, the nanoparticle suspensions were centrifuged at 15,000 rpm for 40 min at 4 °C to ensure complete separation of the nanoparticles using a high-speed cooling centrifuge (HERMLE, Type: Z32HK, Germany). The clear supernatant was carefully collected immediately after centrifugation and analyzed using UV-Vis spectrophotometry. Blank chitosan nanoparticles were prepared under identical conditions in the absence of drug, and their corresponding supernatant was used as the blank to eliminate any background interference. The concentration of the unencapsulated (free) drug in the supernatant, which inherently contained DMSO from the preparation process, was calculated using the corresponding calibration curves, and dilution factors were considered where applicable.

The encapsulation efficiency (EE%) was calculated using the following equation:

$$EE\% = \frac{Wt\ (total\ added\ drug) - Ws\ (free\ drug)}{Wt\ (total\ added\ drug)} \times 100$$

where Wt is the total concentration of the drug used, and Ws is the drug concentration in the supernatant (unentrapped).

Measurements were performed in triplicate (values are expressed as mean ± SD) and carried out under identical experimental conditions to ensure reliability and reproducibility.

2.3. Determination of drug loading percent (DL%)

The drug loading (DL%) of the prepared chitosan nanoformualtions was determined using a direct quantification method.[4] After CNPs preparation, the drug-loaded nanoparticles were separated from the unencapsulated (free) drug via centrifugation (at 15,000 rpm for 40 minutes at 4 °C) using a high-speed cooling centrifuge (HERMLE, Type: Z32HK, Germany), followed by three washes with deionized water. The resulting pellet was lyophilized to obtain the dried drug-loaded formulation. A precisely weighed amount of the dried powder was dissolved in DMSO to disrupt the carrier matrix and fully release the encapsulated drug. The solution was sonicated for 30

minutes and filtered through a 0.22 μm membrane filter. The drug concentration in the resulting solution was determined using UV-Vis spectrophotometry against a standard calibration curve. The DL% was then calculated using the following equation:

$$DL\% = \frac{Weight\ of\ drug\ in\ nanoparticles}{Total\ weight\ of\ nanoparticles} \times 100$$

Where weight of drug in nanoparticles is the actual weight of the drug that was successfully encapsulated, and total weight of nanoparticles includes the weight of encapsulated drug and weight of carrier.

Measurements were performed in triplicate (values are expressed as mean ± SD) and carried out under identical experimental conditions to ensure reliability and reproducibility.

3. DFT Calculations Data

3.1. Polarizability and Dipole Moment Analysis

The dipole moment and molecular polarizability were computed for compounds **5** and ***E*-6** to quantify their response to electric fields and to predict their capability for intermolecular interactions (**Table S1**). The results show that both compounds exhibit significant polarity and polarizability, consistent with their conjugated π-systems and heteroatom content. Their large, calculated dipole moments of 6.0236 and 8.3571 Debye for **5** and ***E*-6**, respectively, are consistent with the pronounced charge separation observed in the MEP maps. The formation of the imine bond in ***E*-6**, which incorporates an additional electron-deficient 1,2,4-triazole ring, extends the conjugated framework and creates a more pronounced charge separation compared to the aldehyde-containing compound **5**. The results provide a cohesive electronic profile. As indicated earlier, the elevated dipole moment and polarizability of ***E*-6** align with its small HOMO-LUMO energy gap, its distinct electrophilic and nucleophilic regions on the MEP surface, and its role as a strong electron acceptor. The collective data confirms that the structural modification successfully amplified key electronic properties. These enhanced characteristics are significant for applications depending on specific and strong intermolecular binding, such as interactions with biological targets.

Table S1. Calculated polarizability and dipole moment of compounds **5** and ***E*-6**.[a]

Compound	Dipole moment (Debye)				Polarizability (a.u.)
	X-axis	Y-axis	Z-axis	Total	
5	-3.5722	4.8500	-0.0325	6.0236	203.79
***E*-6**	-7.2158	4.2109	-0.2026	8.3571	260.91
a: Dipole moment calculations were conducted along the x, y, and z axes.					

4. Biological Evaluation Procedures

4.1. Antidiabetic activity

4.1.1. *In vitro* α-amylase inhibitory assay [5]

In microtiter plate wells, 10 µL of the tested compounds at serial dilutions (10, 50, 100, 200, and 500 µg/mL), acarbose (positive control) or DMSO (negative control), were mixed with 110 µL of diluted Bovine pancreatin α-amylase (EC 3.2.1.1) at concentration of 5 mg/0.5 mL in 0.1 M phosphate buffer at pH 7.4, further diluted 1:10 with the same buffer. Microtiter plate wells were incubated at 37°C for 30 minutes. Subsequently, 60 µL of dextrin solution (1% w/v in distilled water) was added as the substrate and then incubated at 37°C for 20 min, followed by 100 µL of glucose detection reagent (from the commercial kit, containing phosphate buffer, phenol, 4-aminoantipyrine, glucose oxidase, peroxidase, and sodium azide) was added to all wells. The absorbance of red-violet quinone-imine chromogen was measured at 490 nm with a spectrophotometer. The sample blank (reagents + the tested compound without the glucose detection reagent) was prepared to exclude any interference from the compounds themselves. The α-amylase inhibition activity of the tested compounds was determined using the formula below:

The α-amylase inhibitory of the test compound (%) = $(\frac{AC-AS}{AC})$ *100

Where;

A_C: The mean absorbance of the negative control.

A_S: The mean absorbance of the test compound - the mean absorbance of the test blank.

100: Multiplication factor to represent the percentage of inhibition.

The α-amylase inhibition activity of the test compound was expressed as IC_{50} (µg/mL) (the inhibitory concentration required to inhibit 50% of α-amylase activity) and conducted in triplicate, with values ± standard deviation (SD) and determined graphically from a non-linear regression curve of percent inhibition versus concentration using GraphPad Prism 10.

4.1.2. *In vitro* α-glucosidase inhibitory assay [6]

In microtiter plate wells, 10 µL of the tested compounds at serial dilutions (10, 50, 100, 200, and 500 µg/mL), acarbose (positive control) or DMSO (negative control), were mixed with 110 µL of diluted *Saccharomyces cerevisiae* glucosidase (EC 3.2.1.20) at concentration of 5 mg/0.5 mL in 0.1 M phosphate buffer at pH 7.4, further diluted 1:10 with the same buffer. Microtiter plate wells were incubated at 37°C for 30 minutes. Subsequently, a volume of 50 µL of 1 mM *p*-nitrophenyl-D- glucopyranoside (*p*NPG) was added as the substrate. Following incubation at 37°C for 30 min, the reaction was terminated by adding 50 µL of sodium carbonate (0.25 M). Enzymatic activity was quantified by measuring the absorbance at 410 nm. The sample blank (reagents + the tested compound without *p*NPG substrate) was prepared to exclude any interference from the compounds themselves.

Inhibition (%) was calculated as: $(\frac{AC-AS}{AC})$ *100

The α-glucosidase inhibition activity of the test compound was expressed as IC_{50} and conducted in triplicate, with values ± standard deviation (SD). The IC_{50} values (µg/mL) were determined from a non-linear regression curve of percent inhibition versus concentration using GraphPad Prism 10.

4.1.3. *In vitro* glucose uptake assay [7]

A modified yeast cell model was employed to assess glucose uptake enhancement. Baker's yeast (*Saccharomyces cerevisiae*) was washed and centrifuged (3000 × g, 5 minutes) to prepare a 10% (v/v) suspension in distilled water. In separate tubes, 1 mL of the tested compounds at serial dilutions (10, 50, 100, 200, and 500 µg/mL), berberine (positive control), or DMSO (negative control) was added to 1 mL of glucose solution (25 mM in distilled water) and incubated for 10 minutes at 37 ℃. Subsequently, 100 µL of yeast suspension was added, and incubation continued for 60 minutes at 37 °C. Tubes were centrifuged (2500 × g, 5 minutes) to pellet the yeast cells. The residual glucose in the supernatant was quantified using a glucose oxidase-peroxidase (GOD-POD) assay kit (phosphate buffer was added to the sample blank tube).

The glucose uptake of the tested compounds was estimated from the following formula:

The glucose uptake of compounds (%) = $(\frac{AC-AS}{AC})$ *100

Where;

A_C: The mean absorbance of negative control.

A_S: The mean absorbance of test compound - the mean absorbance of test blank.

100: Multiplication factor to represent the percentage of enhancement.

EC_{50} values were determined from a non-linear regression curve of percent glucose uptake versus concentration using GraphPad Prism 10. One way ANOVA test was used for comparing the different studied groups and followed by Post Hoc test (Tukey) for pairwise comparison. The EC_{50} value is the concentration at which glucose absorption is stimulated by 50%.

To exclude potential interference of the chitosan nanoparticles with absorbance or assay readouts, appropriate nanoparticle blank controls were included. For the α-amylase and α-glucosidase inhibition assays, different concentrations of nanoparticles were mixed with the substrate and the color-developing reagent under identical conditions but without enzyme. The absorbance of these nanoparticle blanks was measured, and any detectable signal was subtracted from the corresponding reaction readout when interference was observed. If no interference was detected, no correction was applied.

4.2. Antioxidant activity

4.2.1. Nitric oxide (NO) scavenging activity [8]

The NO radical scavenging activity was evaluated by measuring the inhibition of nitrite formation generated from sodium nitroprusside. Briefly, in a 96-well plate, 50 µL of the tested compounds at serial dilutions (10, 50, 100, 200, and 500 µg/mL) were mixed with 100 µL of sodium nitroprusside (10 mM in 0.1 M sodium phosphate buffer, pH 7.4) and incubated at 25°C for 90 minutes. Following incubation, 100 µL of Griess reagent (prepared by mixing equal volumes of 1% (w/v) sulfanilamide in 2.5% H_3PO_4 and 0.1% (w/v) NEDA in 2.5% H_3PO_4) was added to each well. The absorbance was measured at 546 nm after a 10-minute incubation at room temperature. Ascorbic acid served as positive control at the same serial dilutions. The percentage of NO scavenging activity was calculated as:

$$\text{Inhibition (\%)} = \left(\frac{AC-AS}{AC}\right) *100$$

Where;

A_C: The mean absorbance of the negative control.

A_S: The mean absorbance of test compound - the mean absorbance of test blank.

100: Multiplication factor to represent the percentage of enhancement.

The half-maximal inhibitory concentration (IC_{50}) was conducted in triplicate, with values ± standard deviation (SD). The IC_{50} values (µg/mL) were determined from a non-linear regression curve of percent inhibition versus concentration using GraphPad Prism 10.

4.2.2. 2,2′-Diphenyl-1-Picrylhydrazyl (DPPH) radical scavenging activity [9]

The free radical scavenging potential was assessed using the stable DPPH radical, based on the compound's ability to donate an electron to reduce the purple $DPPH^{\bullet}$ to its yellow, non-radical form. Briefly, 100 µl of DPPH solution (0.1 mM in methanol) was mixed with incubated with 100 µl of serial diluted compounds or ascorbic acid (reference standard, 10, 50, 100, 200, and 500 µg/mL) in a 96-well microplate. The mixture was incubated for 30 minutes at room temperature in the dark. The absorbance was then measured at 510 nm. The percentage of DPPH radical scavenging activity was calculated according to the following equation:

$$\text{Inhibition (\%)} = \left(\frac{AC-AS}{AC}\right) *100$$

Where;

A_C: The mean absorbance of the negative control.

A_S: The mean absorbance of test compound - the mean absorbance of test blank.

100: Multiplication factor to represent the percentage of enhancement.

The half-maximal inhibitory concentration (IC_{50}) was conducted in triplicate, with values ± standard deviation (SD). The IC_{50} values (μg/mL) were determined from a non-linear regression curve of percent inhibition versus concentration using GraphPad Prism 10.

To exclude potential interference of the chitosan nanoparticles with absorbance or assay readouts, appropriate nanoparticle blank controls were included. For nitric oxide (NO) measurements, nanoparticles were incubated with the Griess reagent alone, and the resulting absorbance was used as a nanoparticle blank control. In the DPPH antioxidant assay, the absorbance of nanoparticles mixed with DPPH was measured immediately at time zero (prior to incubation) to account for any intrinsic absorbance or light-scattering effects of the nanoparticles. This value was considered during data analysis to ensure that the recorded activity was not influenced by nanoparticle interference.

4.3. *In vitro* drug release study

The *in vitro* drug release study has been performed according to the reported procedure.[10] The *in vitro* release profiles of nanoformulations **5*** and **6*** were evaluated using dialysis bags (Visking® 36/32, 21 mm, MWCO 12,000 -14,000; Serva, Heidelberg, Germany). The membrane was presoaked overnight to be equilibrated before the addition of a specific volume from the formulation. A 1 mL sample from each formulation, equivalent to 0.35 mg was placed into dialysis bags, which were then submerged in beakers containing 50 mL of phosphate buffer (pH 2.0 and pH 7.4) serving as dissolution media. The beakers were maintained at 37 °C ± 0.5°C in a thermostatic shaking water bath at 100 rpm throughout the experiment. At predetermined time intervals (1, 3, 5, 7, 10, 24, and 48 h), 1 mL samples were withdrawn periodically from the dissolution medium and immediately replaced with an equal volume of fresh buffer to maintain sink conditions. The concentration of released drug in each sample was determined spectrophotometrically λ_{max} = 283 for compound **5** and 305 nm for compound **6** against a corresponding blank buffer solution. The percentage of drug released at different time intervals was plotted to determine the drug release profiles for each formulation and pH condition.

4.4. Statistical analysis

All *in vitro* experiments were conducted in triplicate, and data are expressed as mean ± standard deviation (SD). Data normality was assessed using the Shapiro-Wilk test. For comparisons involving equal variances, one-way analysis of variance (ANOVA) followed by Tukey's post-hoc test for pairwise comparisons was applied. Where the assumption of homogeneity of variances was violated (as assessed by Levene's test), Welch ANOVA followed by Games-Howell post-hoc test was used. A p-value < 0.05 was considered statistically significant. All statistical analysis was performed using IBM SPSS Statistics (version 27.0; IBM Corp., Armonk, NY, USA). IC_{50} and EC_{50} values were calculated by non-linear regression analysis using GraphPad Prism (version 10; GraphPad Software, San Diego, CA, USA).

5. *In-silico* Studies

5.1. Molecular Docking Studies

5.1.1. Ligand preparation

The 3D structures of the target compounds **5** and **6** were built and geometry-optimized using the Avogadro software package. Energy minimization was performed using the MMFF94 force field to generate low-energy conformers. Ligands were subsequently prepared for docking using AutoDockTools (ADT) version 1.5.6, where rotatable bonds were detected, non-polar hydrogens were added, and Gasteiger partial charges were assigned to generate the requisite PDBQT files.

5.1.2. Protein preparation

High-resolution crystal structures were retrieved from the RCSB Protein Data Bank (PDB). The selected molecular targets included pancreatic α-amylase (PDB ID: 4GQR), α-glucosidase (PDB ID: 5NN5), GLUT-4 (PDB ID: 7WSM), and the Keap1-Nrf2 complex (PDB ID: 6TYM). All protein structures were prepared using AutoDockTools. Preparation steps included the removal of water molecules, heteroatoms, and native co-crystallized ligands. Polar hydrogen atoms were added, and Kollman united-atom charges were assigned. The prepared structures were then saved in PDBQT format for subsequent molecular docking studies.

5.1.3. Docking protocol [11]

Molecular docking simulations were executed using AutoDock 4.2. A grid box with dimensions of 60 × 60 × 60 and a spacing of 0.375 Å was centered on the binding site residues defined by the native co-crystallized ligand of each target. The conformational search was performed using the Simulated Annealing algorithm with 100 independent runs and 200 cycles per ligand to ensure exhaustiveness.

5.1.4. Validation and consensus scoring

To verify the reproducibility of the docking protocol, a redocking study was performed where the native co-crystallized inhibitors were extracted and re-docked into their respective binding sites. The Root Mean Square Deviation (RMSD) between the re-docked pose and the experimental conformation was calculated; an RMSD below or near 2 Å was considered indicative of a reliable docking protocol. Furthermore, to validate the scoring reliability, a consensus docking assessment was performed using the SwissDock web server (https://www.swissdock.ch/) comparing the binding modes and affinity trends with those obtained from AutoDock.

As presented in **Table S2** and **Figure S9,** the protocol exhibited high fidelity across all targets, with calculated RMSD values ranged from 0.31 Å to 1.73 Å. Since all values are well below the accepted threshold of 2.0 Å, the method was confirmed to be robust and capable of accurately reproducing the bioactive conformations of the ligands within the binding pockets. Notably, the KEAP1-NRF2 system (PDB ID: 6TYM) showed the highest precision with an RMSD of 0.31 Å, while pancreatic α-amylase (PDB ID: 4GQR) showed the highest deviation (1.73 Å).

Table S2. Redocking of Protein targets.[a]

Protein target	PDB ID	Co-crystallized Ligand (Ref)	RMSD (Å)
Pancreatic α-amylase	4GQR	Myricetin	1.73
α- Glucosidase	5NN5	1-deoxynojirimycin	1.098
GLUT-4	7WSM	cytochalasin B	0.75
KEAP1	6TYM	CHEMBL4635041	0.31

a: GLUT-4, glucose transporter 4; KEAP1: Kelch-like ECH-associated protein 1; RMSD: Root Mean Square Deviation.

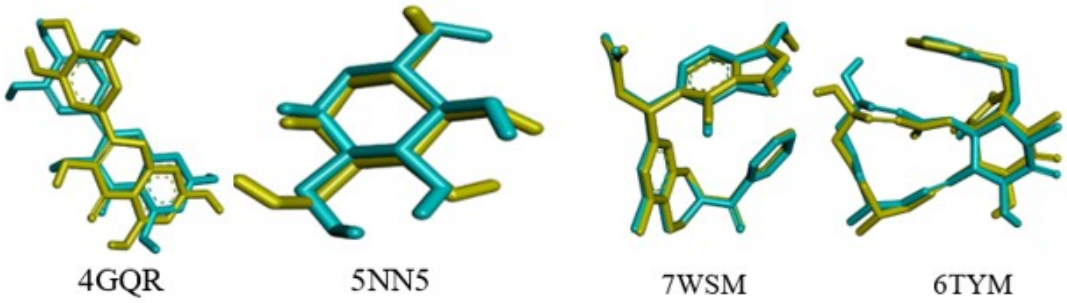

Figure S9. Molecular redocking of each co-crystallized ligand into its protein target, (Yellow, Redocked Co-crystallized ligand; Cyan, Native Co-crystallized ligand).

5.2. Pharmacokinetics and drug-likeness profile

As mentioned in the article, the *in silico* ADME (Absorption, Distribution, Metabolism, Excretion) profiles of compounds 5 and 6 were predicted using the SwissADME and pkCSM web tools. Both compounds exhibit favorable drug-like properties, with high predicted gastrointestinal absorption, no violations of Lipinski's rule of five, and satisfactory scores across multiple drug-likeness filters (Ghose, Veber, Egan, Muegge). Key distinctions include the ability of 5 to cross the blood-brain barrier (BBB permeant = Yes) and its broader cytochrome P450 (CYP) inhibition profile, whereas 6 is a P-glycoprotein substrate and shows more selective CYP inhibition. Neither compound triggered PAINS (pan-assay interference) alerts, though each showed one BRENK alert (aldehyde in **5**, imine bond in **6**). The synthetic accessibility scores indicate that both hybrids are synthetically feasible, with 5 being moderately easier to prepare. These computational predictions support the potential of both hybrids as orally bioavailable drug candidates with suitable pharmacokinetic starting points for further development. The results are summarized in **Table S3**.

Table S3. Predicted pharmacokinetic and drug-likeness profile of **5** and **6**.[a]

Parameter	5	6
GI absorption	High	High
BBB permeant	Yes	No
P-gp substrate	No	Yes
CYP1A2 inhibitor	Yes	No
CYP2C19 inhibitor	Yes	No
CYP2C9 inhibitor	Yes	Yes
CYP2D6 inhibitor	Yes	No
CYP3A4 inhibitor	Yes	Yes
Log Kp (cm/s)	-6.48	-7.05
Lipinski's violations	0	0
Ghose, Veber, Egan, Muegge	Satisfied	Satisfied
Bioavailability score	0.55	0.55
PAINS alerts	0	0
BRENK alerts	1 (aldehyde group)	1 (imine bond)
Lead likeness violations	1 (MWt >350)	1 (MWt >350)
Synthetic Accessibility	2.82	3.33

a: GI, gastrointestinal; BBB, Blood-Brain Barrier; P-gp, P-glycoprotein; CYP, Cytochrome P450; Log Kp, skin permeation coefficient; Ghose, Veber, Egan, Muegge, the four complementary drug-likeness filters; PAINS, Pan-Assay Interference compounds; BRENK, Brenk, Reiller, Netter, Kier.

6. References

1. H. Zhai, C. Luo, P. Yang, S. Zhang, H. Wang, Y. Cao, Y. Yang, H. Liu, X. Kong, F. O. Arhema Frejat, C. Ren, X. Shi and C. Wu, *Eur. J. Med. Chem.*, 2022, **238**, 114495.
2. A. H. Banday, S. A. Shameem, B. Gupta and H. S. Kumar, *Steroids*, 2010, **75**, 801-804.
3. E. Piacentini, in *Encyclopedia of Membranes*, eds. E. Drioli and L. Giorno, Springer Berlin Heidelberg, Berlin, Heidelberg, 2016, https://doi.org/10.1007/978-3-662-44324-8_1945, pp. 706-707.
4. J. Yan, Z.-Y. Guan, W.-F. Zhu, L.-Y. Zhong, Z.-Q. Qiu, P.-F. Yue, W.-T. Wu, J. Liu and X. Huang, *Pharmaceutics*, 2020, **12**, 216.
5. V. K. Kumar and K. G. Lalitha, *Indian J. Pharmacol.*, 2014, **46**, 350-351.
6. T. Matsui, C. Yoshimoto, K. Osajima, T. Oki and Y. Osajima, *Biosci. Biotechnol. Biochem.*, 1996, **60**, 2019-2022.
7. V. S. Madiwalar, P. S. Dwivedi, A. Patil, S. M. Gaonkar, V. J. Kumbhar, P. Khanal and B. Patil, *J Diabetes Metab Disord.*, 2022, **21**, 429-438.
8. E. Mfotie Njoya, A. M. Munvera, P. Mkounga, A. E. Nkengfack and L. J. McGaw, *BMC Complement. Altern. Med.*, 2017, **17**, 199.
9. S. A. Adebayo, M. Ondua, L. Shai and S. Lebelo, *J. Inflamm. Res.*, 2019, 195-203.
10. S. M. Elkarray, R. M. Farid, M. M. Abd-Alhaseeb, G. A. Omran and D. A. Habib, *J. Drug Deliv. Sci. Technol.*, 2022, **68**, 103086.
11. N. El-Hachem, B. Haibe-Kains, A. Khalil, F. H. Kobeissy and G. Nemer, in *Neuroproteomics: Methods and Protocols*, Springer, 2017, pp. 391-403.